Scientific Research Publishing

Open Journal of Applied Sciences, 2021, 11, 294-311
https://www.scirp.org/journal/ojapps
ISSN Online: 2165-3925
ISSN Print: 2165-3917

Performance of Incoming Solar Radiation Components in Partial Annular Solar Eclipse on June 21st, 2020 in Helwan, Egypt

Samy A. Khalil, A. H. Hassan, U. Ali Rahoma, A. Abulwfa, Ashraf S. Khamees

National Research Institute of Astronomy and Geophysics, Helwan, Egypt
Email: samynki@yahoo.com

How to cite this paper: Khalil, S.A., Hassan, A.H., Rahoma, U.A., Abulwfa, A. and Khamees, A.S. (2021) Performance of Incoming Solar Radiation Components in Partial Annular Solar Eclipse on June 21st, 2020 in Helwan, Egypt. *Open Journal of Applied Sciences*, **11**, 294-311.
https://doi.org/10.4236/ojapps.2021.113022

Received: January 22, 2021
Accepted: March 15, 2021
Published: March 18, 2021

Abstract

Observing and studying the solar radiation during solar eclipses is important in knowing the changes that occur to the environmental elements during this event. The main objective of this paper is the performance of the incoming variation of solar radiation components, global, direct and diffuse and their fractions during the partial annular solar eclipse on June 21st, 2020 in Helwan, Egypt (Lat. 29.866˚N and Long. 31.20˚E) has been made. A pyrheliometer for measuring the direct solar radiation, in three different bands; direct yellow (*Y*), direct red (*R*), direct infrared (*IR*), and also the total direct band (*I*); A pyranometers for measuring the different components of global solar radiation (*G*), global ultraviolet (G_{UV}), global infrared (G_{IR}) and a meteorological station to measure the different meteorological parameters. The duration of the solar eclipse was 01 h:59 m, and the maximum magnitude of the eclipse in this region was 0.449. The depression is clear at the solar radiation of all components due to the annular solar eclipse, while the depressions of the diffuse and global infrared solar radiation are lower. In all direct radiation compounds (*I*, *Y*, *R* and *IR*) are greatly affected by the eclipse. The diffuse fraction K_d is higher in the early time, before the partial eclipse, but during the partial annular eclipse time K_d values are suffers variation and through the day, where the values of K_d lies between K_t and K_{UV}. The values of direct infrared solar radiation are dominant before and after the partial annular solar eclipse. The intensity of color bands ($W \cdot m^{-2} \cdot nm^{-1}$) are *DIB*3 > *DIB*2 > *DIB*4, and *DIB*1 is opposite direction with *DIB*3 and *DIB*2, the highest intensity is direct red and the lowest intensity is the direct infrared. The highest values of extinction coefficient in (G_{IR}) solar radiation and the lowest values occur in (G_{UV}) solar radiation, while the values of (*G*) solar radiation occur between them. In general trend, the values of extinction coefficient during the partial eclipse are increasing, while the minimum values of extinction coefficient occur at noon time due to the air mass is less value in the noon.

Keywords

Solar Radiation Components, Annular Solar Eclipse, Color Portion, Transparency and Link and Angstrom Turbidity

1. Introduction

A solar eclipse is a natural event that takes place on Earth when the Moon moves in its orbit between Earth and the Sun (this is also known as an occultation). Solar eclipses provide an unusual opportunity to study a rapid and well-characterized change in the solar radiation entering the atmosphere. While radiation measurements related to eclipse changes have been made at the Earth's surface [1] [2] [3]. A total solar eclipse occurs when the Moon completely blocks the solar disk. In a total solar eclipse, the narrowest part of the path (where the Sun is completely blocked and the Moon casts its darkest shadow (called the umbra)) is called the "zone of totality". Total solar eclipses have not always been visible from Earth. When the Moon is farther away in its orbit than usual, it appears too small to completely cover the Sun's disk. During such an event, a bright ring of sunlight shines around the Moon. This type of eclipse is called an "annular" or "partial" eclipse. It comes from the Latin word "annulus" which means "ring" [4] [5]. Partial and total solar eclipses have been the exclusive concern of Astronomy and Astrophysics. The greatest eclipse is defined as the instant when the axis of the Moon's shadow passes closest to the Earth's center. For the total eclipses, the instant of greatest eclipse is virtually identical to the instants of greatest magnitude and greatest duration. However, for annular eclipses, the instant of greatest duration may occur either at the time of greatest eclipse or near the sunrise and sunset points of the eclipse path [6]. On Saturday June 21st, 2020 in Helwan, Egypt, a partial annular solar eclipse of the Sun was visible from within a narrow cored or which traversed half the Earth. The partial solar eclipse was started at 06:23:09, the maximum eclipse will occur at 07:19:29 when the Sun reaches an altitude of 29.866˚ and azimuth of 078˚; this event will come to an end at 08:22:20 and will have a magnitude of 0.457 (the magnitude of an eclipse is the ratio of the apparent size of the Moon to the apparent size of the Sun during an eclipse), and an obscurity of 0.343 (the fraction of the Sun obscured).

Many several studies claiming of the variation of solar radiation and transparency has been carried out in recent years, dealing with solar eclipse totality and partiality in different countries. The around about this subject was carried out in the world, especially in this region. In Romania, a study of atmospheric responses due to August 11th, 1999 total solar eclipse indicated that both of the global and UVB radiation dropped dramatically to a minimum around totality. There was a chance to study attenuation of such a radiation due to clouds [7] [8] [9]. The concluding indicated that there is an increase in the hole with different zonal summer times in the interval 350 - 450 nm but without risks on the human

eye, that interval lied at the end of the ultraviolet solar radiation, minimum lied from 500 - 700 nm. This interval represented the normal maximum peak of the solar spectrum and go from 700 nm up to 900 nm, which related to the infrared interval and down in the deep infrared from 900 nm to the end. The ultraviolet band was suffering low depression with respect to other bands, but was not given any risks on the human life as common [10] [11] [12] [13] [14]. A study was made of the depression of the different solar radiation components during the solar eclipse, August 11th, 1999, over Egypt (as a partial solar eclipse, 70% covering of the solar disk in Helwan, Egypt). The maximum depression values of the different components of solar radiation were 54% in red solar radiation (for global and direct), while the minimum depression was in infrared solar radiation (34% for global and 41% for direct). The clearness index and the diffuse fraction were 0.634 and 0.232, respectively. The atmospheric red radiation was 7.4% and the atmospheric infrared radiation was 10.7%. The percentage of ultraviolet was 3%. A study of the spectral composition of global solar radiation by interference metallic filters was carried out during the same previous eclipse on August 11th, 1999 in Helwan, Egypt [15].

A Solar eclipse is one of the most spectacular astronomical phenomena which occur when the Moon covers the Sun, casting its shadow on the Earth a dating spires meteorologist to conduct special investigations. Eclipses are connected with the rapid and short time, impulse-like decrease of the solar energy flux reaching the area of its visibility, which can be exactly predicted before the occurrence of the phenomenon. It also provides a unique opportunity for meteorology is to study the response of the atmosphere or biosphere to the sudden turn off/turn on of the incidental solar radiation during and after the solar eclipse [16] [17] [18]. There are a number of studies and observations made during the solar eclipses, which include observations of meteorological parameters, such as wind speed and direction, air temperature, atmospheric pressure, humidity, ozone measurements and heat and momentum fluxes within the boundary layer [6] [19] [20]. The impact of a solar eclipse on atmospheric and surface temperature has been widely reported changes in wind speed during the eclipse with a minimum value during totality but without much change in wind direction. Observed sharp increases in the UV flux after the last two hours of contact of the eclipse on 24 October, 1995, these authors attributed the observed increases in ground-based UV flux to the reduction of stratospheric ozone [21].

Solar eclipse episodes are often favorable opportunities for closely observing the effects of interactions between solar irradiance and the terrestrial atmosphere, studies on this topic can be very useful for testing and improving the radiated transform models used to simulate the spectrum of ultraviolet (UV) solar irradiance reaching the surface [22] [23] [24]. In addition, the solar radiation partly reflected upward from the surface or by cloud scan be scattered by air molecules and aerosols, sometimes enhancing considerably the incoming diffuse radiance flux measured at the observation site. Since Rayleigh scattering closely depends on wavelength, the diffuse radiance is comparable to, or may become

even more intense than the direct component of UV wavelengths, with significantly lower values at the longer wavelengths in the visible and near-infrared spectral ranges. Depending strongly on the atmospheric turbidity conditions and surface reflectivity characteristics, UV diffuse radiance can vary greatly as a function of the environmental parameters. These dependence features have been the subject of numerous studies. The absorbing components of the atmosphere are O_2, O_3, H_2O, CO_2, N_2, O, N, NO, N_2O, CO, CH_4 and their isotopic modifications, though the contributions of the latter are small spectra due to electronic transitions of molecular and atomic of O, N, O_3, lie chiefly in the UV region, while those due to the vibration and rotation of polyatomic molecules such as H_2O, CO_2 and O_3, lie in the IR region. The Angstrom turbidity (β) typically ranges from 0.02, for low aerosol load, to 0.5, for high aerosol load [11] [25] [26] [27]. The main objective of the study is the performance and determines the percentage of color portion, variations of the different solar radiation components in Partial Annular Solar Eclipse on June 21st, 2020 in Helwan, Egypt.

2. Sit Observation and Measurements

Helwan site is selected on a hilltop of height 130 m above sea level (29˚52'N & 30˚20'E) at a distance of about 30 km South of Cairo in a desert surrounding in the East and the Nile valley (cultivated land) in the West. The western desert exists in the far west, where Saqqara and Dahshur Pyramids can be seen under good conditions of visibility. The observation conditions at this site are suffering now from the existence of strong pollution sources in the West (Helwan Town, Portland Cement Company and a power Station), Southwest. Equipment was installed on the roof of the National Research Institute of Astronomy and Geophysics (NRIAG) building in Helwan, the background is taken as desert and pollution.

The average concentration of total suspended particulates (TSP) is ranged 500 - 600 μg/m^3. Tura EL-Cement and Helwan Portland cement factories were found to represent 50% of the pollution sources in Helwan region. XRD (X-ray diffraction) patterns of $PM_{2.5}$ samples are ($CaSO_4{\cdot}H_2O$, $Al_2Si_2O_5(OH)_4$, SiO_2, $CaCO_3$ and $CaMg(CO_3)_2$, Fe_2O_3, NaCl) respectively. The elements follows the trend as Si > Ca > Ba > Al > K > Zn > Na > Mg > Fe > CL > S > Ni > Ti, P > Sr > Cu. The XRF (X-Ray Fluorescence) and XRD analyses for lead differ somewhat more, being 44 and 2.2%, respectively [28]. The instruments used in the present research (see **Table 1**), and a meteorological station (Davis vantage pro 26,152 weather stations) to measure the different meteorological parameters.

The data collection by the computerized data logger for the different global component and the meteorological parameters, while for the different direct components are taken by the manual.

The extraterrestrial solar radiation (G_o, I_o, Y_o, R_o and IR_o) and the terrestrial solar radiations (G, G_{UV}, G_{IR}, I, Y, R and IR) calculated by W/m^2 are defined bands as:

Table 1. The instruments of solar radiation measurements used in the work.

Type	Solar radiation	Symbol	Company
pyranometers	Global	G and G_{IR}	EPPLEY
pyrheliometer	Direct	I, Y, R, IR	EPPLEY
pyranometers	Diffuse	D	KIPP & ZONEN CMP10
pyranometers	UV	G_{UV}	Midlltone

G_o, G and I = 280 - 2800 nm, UV_o and G_{UV} = 285 - 385 nm, Y_o and Y = 530 - 2800 nm, R_o and R = 630 - 2800 nm, IR_o and IR = 695 - 2800 nm.

The color intensity bands, Bi (W/m^2) calculated as: $IB1 = I - Y$ = 280 - 530 nm, ΔB1 = 250 nm, $IB2 = Y - R$ = 530 - 630 nm, $\Delta B2$ = 100 nm, $IB3 = R - IR$ = 630 - 695 nm, $\Delta B3$ = 65 nm, $IB4 = IR$ = 695 - 2800 nm, $\Delta B4$ = 2105 nm.

The color intensity bands, $DIBi$ (W·m^{-2}·nm^{-1}) calculated as: $DIB1 = IB1/\Delta B1$ (W·m^{-2}·nm^{-1}), $DIB2 = IB2/\Delta B2$ (W·m^{-2}·nm^{-1}), $DIB3 = IB3/\Delta B3$ (W·m^{-2}·nm^{-1}). $DIB4 = IB4/\Delta B4$ (W·m^{-2}·nm^{-1}).

The color portion bands, $DCBi$ (% or ratio·nm^{-1}) calculated as: $DCB1 = DIB1/I$, $DCB2 = DIB2/I$, $DCB3 = DIB3/I$ and $DCB4 = DIB4/I$ (% or ratio·nm^{-1}).

Global event of the partial annular solar eclipse at 21 June 2020 at Helwan and the eclipse duration is 01 h:59 m (see Table 2).

Mie's theory and Rayleigh's classified the size particle of a scattering as the function in the wavelength λ as: $\pi d/\lambda$, where d is the particle diameter. Let n be the index of refraction and λ the wavelength in micrometers. It is considered that, 1) when $\pi d/\lambda < 0.6/\pi$, scattering is governed by Rayleigh's theory, and in a cloudless atmosphere applies to air molecules, most of which have a size ≈ 1 Ä; 2) when $\pi d/\lambda > 5$, scattering is chiefly a diffuse reflection process seldom occurring in the earth's atmosphere; and 3) when $0.6/n < \pi d/\lambda < 5$, scattering is governed by Mie's theory, and applies to scattering by particles of size greater than 10 Ä, such as aerosols [11].

3. Methodology

During the overshadowing, the solar radiation is diminished from that normal for a similar area and season, by the extent of the sun powered circle's territory covered (the obscuration). Ascertaining the solar radiation during the overshadowing can be accomplished by consolidating the standard count of the everyday variety in top-of-air sun powered radiation with a regulating capacity to speak to the shroud. The highest point of-air sun powered radiation is basically a cosmic count: the genuine radiation in the lower environment will be decreased from the highest point of-air and incentive through ingestion by ozone and water fume, which is variable. Expecting unimportant distinction between the real and mean Sun-Earth separates the time variety in sun powered irradiance on an even surface at the highest point of the climate $S_T(t)$ is given roughly by [27].

$$S_T(t) = S_0 \cos\left[Z(t)\right] \tag{1}$$

Table 2. Phases of the annular partial solar eclipse in Helwan, Egypt 21 June 2020.

Eclipse phases	First contact	Maximum	Last contact
L.M.T, hh:mm	06 h:23 m	07 h:20 m	08 h:22 m
Altitude of the sun, a	16.9˚	28.7˚	42.1˚
Azimuth of the sun, Az	72˚	78˚	84˚
Eclipse magnitude		0.449	

where (S_0) is the total solar irradiance (TSI) and (Z) is the solar zenith angle at a time t. For a site at latitude (φ) when the solar declinations (δ), the variation in (Z) during the day are found from the hour angle $H(t)$ as:

$$\cos\left[Z(t)\right] = \sin\varphi\sin\delta + \cos\varphi\cos\delta\cos H(t) \tag{2}$$

The solar irradiance variation with time at a particular position is conventionally calculated by combining Equations (1) and (2) to give

$$S_T(t) = S_0\left[\sin\varphi\sin\delta + \cos\varphi\cos\delta\cos H(t)\right] \tag{3}$$

On a day with a total solar eclipse, an additional modulation function is needed to represent the effect of the eclipse. The solar irradiance can then be written as [27].

$$S_T(t) = \left[1 - E(t)\right]S_0\left[\sin\varphi\sin\delta + \cos\varphi\cos\delta\cos H(t)\right] \tag{4}$$

where $E(t)$ is the eclipse function which gives as:

$$E(t) = 1 - (2/\pi)\cos^{-1}\left[f_e(t)\right] - (2/\pi)f_e(t)\left\{1 - f_e(t)^2\right\}^{1/2} \tag{5}$$

where $f_e(t)$ is the eclipse magnitude, the proportion of the Sun's radius obscured by the Moon at a time. The extraterrestrial solar radiation at any time during the partial solar eclipse can be calculated as following [25].

$$E_i \text{ at eclipse} = (E_i)(1 - M) \tag{6}$$

where (M) is magnitude of solar eclipse defined as the fraction of the solar diameter that is obscured and E_i is substituted by any radiation quantity, e.g. G_o, G_{IR}, G_{UV}, B_1, B_2, B_3 and B_4. Extinction coefficient (α) calculated by the:

$$I_{b\lambda} = I_{o\lambda}\exp(-\alpha m_A) \tag{7}$$

where ($I_{b\lambda}$) is the measured spectral irradiance at wavelength (λ) and ($I_{o\lambda}$) is the extraterrestrial spectral irradiance corrected for the actual sun-earth distance.

Also we can calculate the extinction coefficient values of (α) as following equation [25]:

$$\alpha = -\ln(I_{b\lambda}/I_{o\lambda})(1/m_A) \tag{8}$$

Air transparency, (T_r),

$$T_r = \mathrm{e}^{-\alpha} \tag{9}$$

The calculations of the extraterrestrial solar radiation for the bands of various components bands are based on [11] [25].

The diffuse infrared (D_{IR}) was calculated from the equation:

$$D_{IR} = G_{IR} - IR\cos(Z) \tag{10}$$

The Linke turbidity factor, LT is given by:

$$L.T. = \left(1/\delta_R m_A\right)\cdot \ln\left(I_o/I\right) \tag{11}$$

where δ_R is given by:

$$\delta_R = 1/\left(9.4 + 0.9 m_A\right) \tag{12}$$

where m_A is relative optical air mass and given by:

$$m_A = \left(P/1013.25\right)\left[\left(1/\cos Z\right) + 0.15\left(93.885 - Z\right)^{-1.25}\right] \tag{13}$$

where, (P) is the air pressure (hpa).

The total amount of water vapor in the atmosphere in the vertical direction is highly variable and depends on the instantaneous local conditions. This amount, expressed as perceptible water W (cm), and can be readily computed through a number of standard routine atmospheric observations. The perceptible water vapor can vary from 0.0 to 5 cm [25] [29].

$$W = \left\{0.493\left(\varphi_r\right)\exp[26.23 - \left(5416/T_k\right)\right\}/T_k \tag{14}$$

where, (T_k) is the ambient temperature in kelvins and (φ_r) is the relative humidity in fraction of one ($\varphi_r = RH/100$).

The Angstrom turbidity coefficient is a dimensionless index that represents the amount of aerosol, and the relation between the Linke turbidity (LT) and the Angstrom turbidity (β) for Helwan is [25] [30]:

$$\beta = -0.194933 + 0.0620059 LT \tag{15}$$

4. Results and Discussion

Figure 1 shows the hourly variation of extraterrestrial solar radiation components bands, global (G_o), ultraviolet (UV_o), yellow (Y_o), red (R_o) and infrared (IR_o) in W/m^2 and it shows the decrease in the solar energy interior in all components.

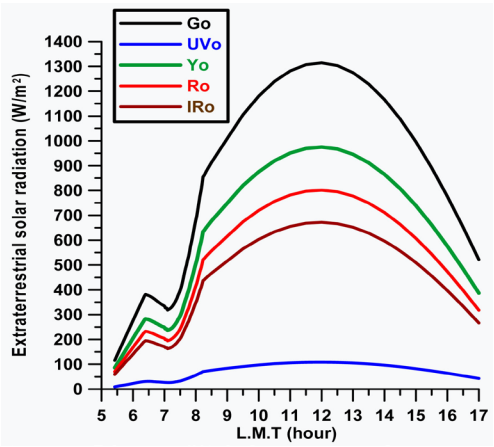

Figure 1. The hourly variation of extraterrestrial solar radiation (W/m^2).

Figure 2 shows the hourly variation measurements of incoming solar radiation components, global (G), global infrared (G_{IR}), diffuse (D) and global ultraviolet (G_{uv}) in W/m^{2}during the day, including the depression of the solar radiation components at the interval of partial annular solar eclipse. From this figure, we noticed that the depression of the solar radiation of all components due to the partial annular solar eclipse, while the depressions of the diffuse and global infrared solar radiation are lower. The behavior of the turbulent diffuse radiation (D) expresses the state of change in the transparency of the atmosphere.

Figure 3 shows the hourly measurements of various direct solar radiation components; total (I), yellow (Y), red (R) and infrared (IR) in W/m^2. This figure pointing to the depression gradient starting from the direct total two infrared bands passing through the yellow and red bands before and after the partial annular solar eclipse, the difference between the bands is narrow during the maximum eclipse. To compare between the global and direct components, in all direct solar radiation compounds (I, Y, R and IR) is greatly affected by the eclipse, while the effect is small in case the total solar radiation compounds (G, G_{uv}, G_{IR} and D).

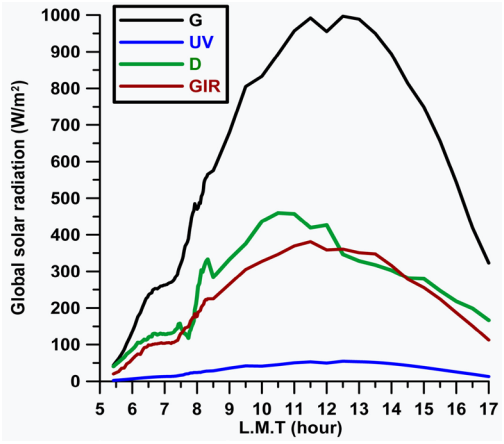

Figure 2. The hourly variation of measured global and diffuse solar radiation (W/m^2).

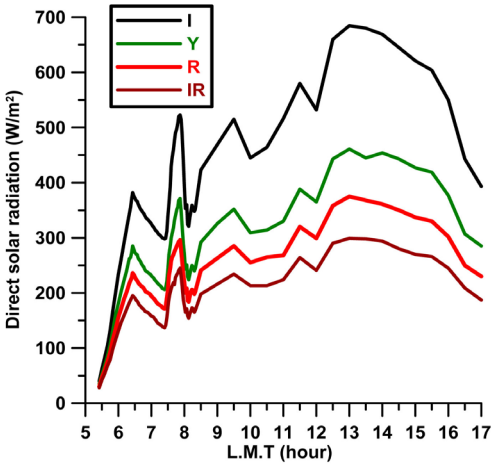

Figure 3. The hourly variation of measured direct solar radiation components (W/m^2).

Figure 4 shows the hourly variation of clearness index for each of the global (K_t), ultraviolet (K_{uv}), and infrared (KG_{IR}) addition to the diffuse fraction (D/G). From this figure, the diffuse fraction K_d is higher in the early time, before the partial eclipse, but during the partial annular eclipse time K_d values are suffers variation and through the day, where the values of K_d lies between K_t and K_{UV}. Where the diatomic oxygen (O_2), nitrogen (N_2), atomic oxygen (O), nitrogen (N), and ozone (O_3) are the five principal absorbers in the ultraviolet and visible spectrum [11]. During the partial annular solar eclipse, the behavior of K_t and K_{UV} are similar, while the (K_d) is opposite direction, this means that the scattered radiation is greater during the eclipse. Also from this figure, the clearness indices have higher values during the partial annular eclipse, but after the partial eclipse, the values of K_t are higher and the values of (K_d) are lowest. The observers notice that by the naked eye there are a light cloud of air pollutants at the altitude of the Sun ($a \approx 50.307^\circ$ - 63.284°).

Figure 5 shows the hourly variation of the horizontal global infrared G_{IR} and the direct infrared IR over the whole day. The IR is predominant outside the partial annular solar eclipse, but these changes during a partial eclipse. The difference between the values of G_{IR} and IR solar radiation is the diffuse infrared solar radiation, where a part of the direct red and infrared radiation are converted into diffuse infrared by the artificial of air pollutants during this period. Figure 6 shows the hourly variation of the irradiance of the total diffuse solar radiation (D) and the diffuse infrared solar radiation (D_{IR}). From this figure, we clear that the total diffuse solar radiation values were higher than the diffuse infrared solar radiation values before, after and during the partial annular solar eclipse. A number of gases absorb solar electromagnetic radiation in the infrared wavelengths; the important absorbers of these gases are H_2O, CO_2, O_3, N_2O, CO, O_2, CH_4, and N_2. The water-vapor bands of importance are at 720, 820, 940, 1100, 1380, 1870, 2700, 3200, and 6300 nm; those of carbon dioxide are at 1450, 1600, 2000, 2700, 4300, 4800, and 5200 nm; and those of oxygen are at 690 nm and 760 nm [11].

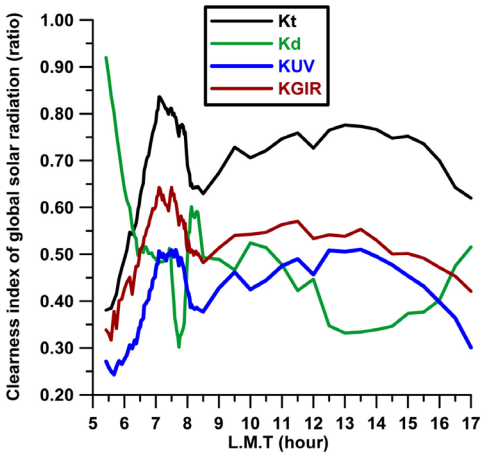

Figure 4. The hourly variation of clearness index for global and diffuse fraction (ratio).

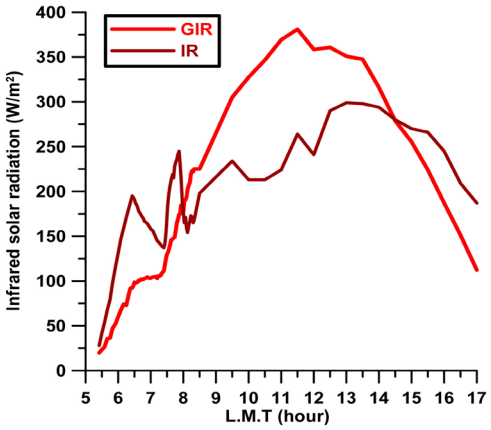

Figure 5. The hourly variation of infrared solar radiation (W/m^2).

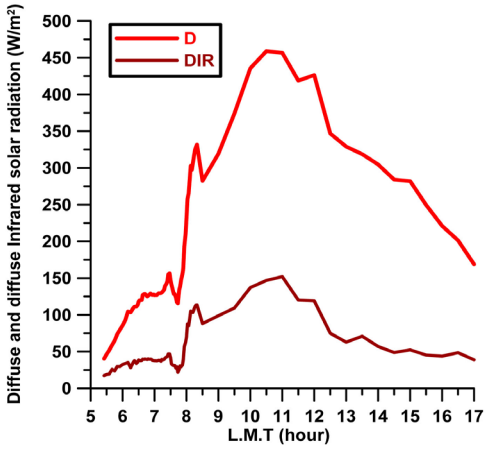

Figure 6. The hourly variation of diffuse and diffuse infrared solar radiation (W/m^2).

Figure 7 shows the hourly variation of the color bands intensity for the direct radiation components of *DIBi* (W·m^{-2}·nm^{-1}) over the whole day. Generally, this figure shows, the intensity of bands are *DIB*3 > *DIB*2 > *DIB*4, *DIB*1 is opposite direction with *DIB*3 and *DIB*2, it turns out that, the highest intensity is direct red and the lowest intensity is the direct infrared.

Figure 8 shows the different percentage of the color portion, *DCBi* (%·nm^{-1}) bands through the day passing during the partial annular solar eclipse. This figure shows that the prevailing color portion bands in the clear case are *DCB*3 > *DCB*2 > *DCB*4, and *DCB*1 is opposite direction with *DCB*3 and *DCB*2, where the high percent of color portion bands generally is the red color (*DCB*3). From **Figure 7** and **Figure 8**, it is similar prevailing in the *DIBi* (W·m^{-2}·nm^{-1}) and *DCBi* (%·nm^{-1}) for all bands, which indicated the band 530 - 630 nm is the largest percent of color portion.

Figure 9 shows the ratio of diffuse infrared solar radiation to the total diffuse solar radiation (D_{IR}/D) with the behavior of magnitude of eclipse, where the maximum ratio occur before and after the partial solar eclipse, while decrease ratio occur during the interval time of solar eclipse. **Figure 10** shows the hourly

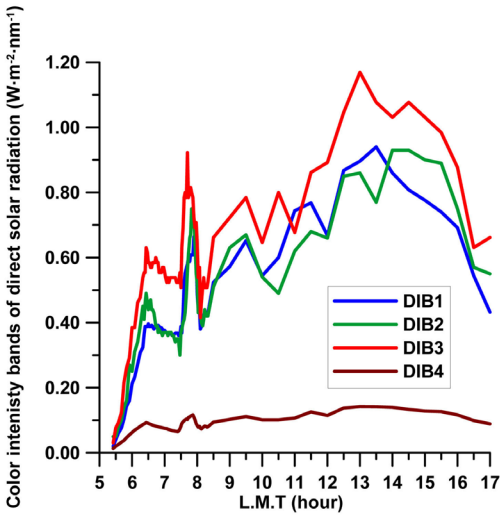

Figure 7. The hourly variation of color intensity bands of direct solar radiation components.

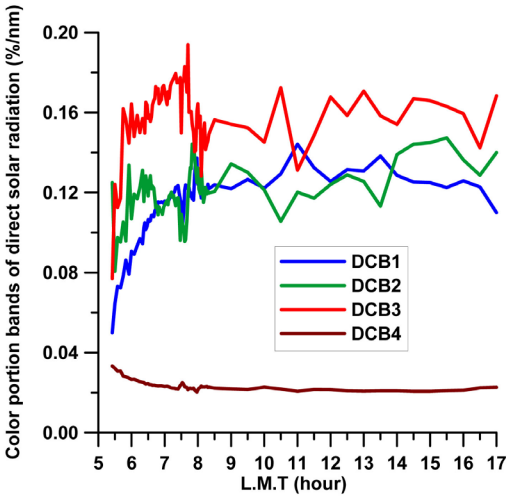

Figure 8. The hourly variation of color portion bands of direct solar radiation components.

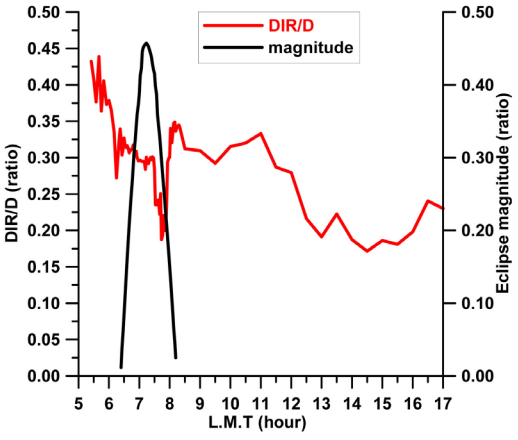

Figure 9. The hourly variation of D_{IR}/D (ratio) with the eclipse magnitude (ratio).

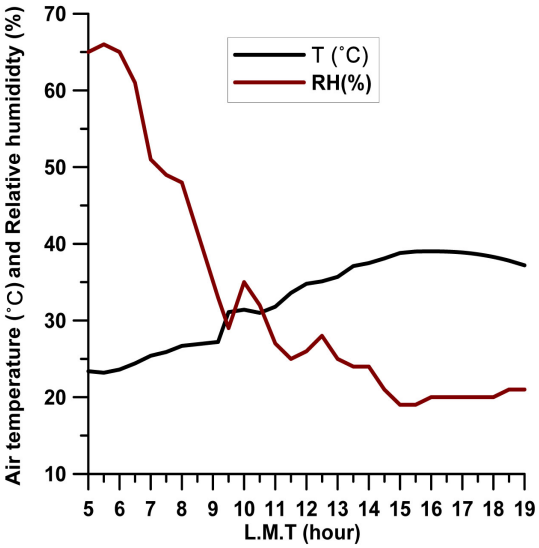

Figure 10. The hourly variation of ambient air temperature (˚C) and relative humidity (%).

variation of air temperature, T (˚C) and RH (%) on the day, where the relation is inversely. **Figure 11** shows the variation of color portion percent bands (%·nm^{-1}) during the eclipse magnitude. The largest percent values occur in the red color ($DCB3$), while the lowest values occur at the infrared color ($DCB4$) and the values of $DCB1$ and $DCB2$ are approximately equal in value. It also notes that the direction and behavior of all colors are in the same phase, unlike the behavior of colors before and after the eclipse.

Table 3 shown the statistical values of the extinction coefficient (E) for each of G, G_{IR}, G_{UV}, I, CB_1, CB_2, CB_3, CB_4 during the day passing the partial annular solar eclipse on 21st June 2020, in addition to the atmospheric transparency (Tr) values calculated from the mean of (E) for the same types of radiation values. From this table, the highest value for transparency is G_{UV} rays and the lowest is CB_2.

Table 4 gives the different values of Link turbidity (LT), Angstrom turbidity (β), and perceptible water (W, cm) during the day passing the through the partial annular solar eclipse. Both Linke and Angstrom turbidity values are higher in the afternoon than in the morning. This is due to the high temperature in afternoon, which expands and excites the gases and the dust in the atmosphere. The distribution of perceptible water (W, cm) gives the concept of the atmospheric character during the partial eclipse. The fluctuation of LT and β beside the W (cm) give an idea of the turbidity of the day observation. The LT and β values are higher in the afternoon than in the morning. This is because of the high temperature in the afternoon, which expands and excites the gases and the fine dust in the atmosphere. During the eclipse (from the first contact to the last contact), the ranged values of the LT, β and W (cm) are 2.02 - 3.12, 0.015 - 0.027 and 3.14 - 2.68 respectively.

Table 3. The statistical values of the extinction coefficient (E) for each of G, G_{IR}, G_{UV}, I, CB_1, CB_2, CB_3, CB_4 during the day passing the partial annular solar eclipse on 21st June 2020, in addition to the atmospheric transparency (Tr) values calculated from the mean of E for the same types of radiation values.

	G	G_{IR}	G_{UV}	I	CB1	CB2	CB3	CB4
Number of values	92	92	92	92	92	92	92	92
Minimum	0.202	0.286	0.129	0.295	0.301	0.308	0.305	0.291
Maximum	0.461	0.559	0.352	0.683	0.734	0.792	0.751	0.671
Range	0.259	0.273	0.223	0.388	0.433	0.484	0.446	0.38
Mean (E)	0.2806	0.3917	0.1838	0.4029	0.4377	0.4776	0.4583	0.3891
SD	0.06771	0.06507	0.06315	0.1099	0.1185	0.1399	0.1282	0.1059
T_r	0.755	0.676	0.832	0.668	0.6455	0.620	0.632	0.677

Table 4. The variation values of link turbidity (LT), Angstrom turbidity (β) and perceptible water (W, cm) during the day passing through the eclipse period.

Time	6:00	6:23 F.C.	7:00	7:19 M.E.	8:00	8:23 L.C.	9:30	10:00	11:00	12:00	13:00	14:00	15:00	16:00	17:00
LT	2.07	2.02	2.83	3.28	3.59	3.12	3.59	3.95	4.25	4.89	4.78	5.29	5.74	5.91	5.31
β	0.012	0.015	0.024	0.028	0.025	0.027	0.034	0.035	0.032	0.042	0.048	0.132	0.167	0.183	0.213
W	3.12	3.14	2.88	2.67	2.68	2.76	2.22	2.38	2.32	2.29	2.38	2.44	2.20	2.17	2.23

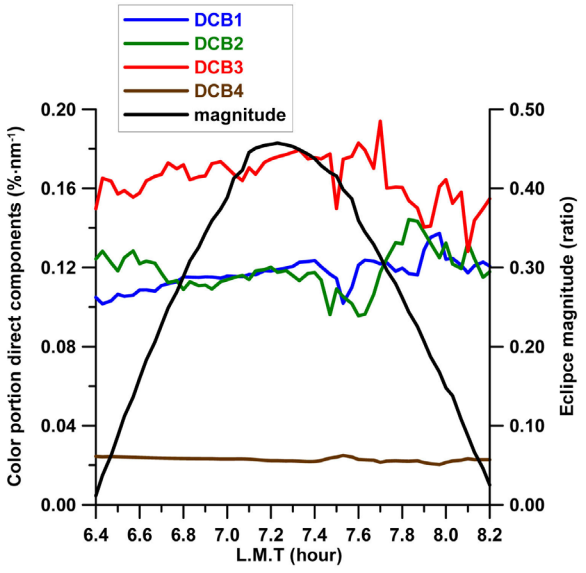

Figure 11. The variations of color portion during the eclipse magnitude (%·nm^{-1}).

Table 5 represents the linear regression [$Y(LT, \beta, W) = a + bX$ (hour)] between the LT, β and W (cm) with the time (hour) and the correlation coefficients (CC) according values of **Table 3**. The rate increase of the LT with time is $dLT/dt = +0.3313$ (high correlate ≈ 0.96), the rate increase of β with the time is $d\beta/dt = +0.01697$, while the rate decrease for the W (cm) with the time is $dW/dt = -0.0751$. It is clear that the relationship is positive with the progression of time with an increase in the intensity of solar radiation and then the direct functions

in the temperature, which leads to an increase in the spread and excitation of the atmospheric air components in a tropospheric region. While the relationship is inverse and indirect in case the perceptible water (W, cm) with the time. This is caused by the average concentration of particulate matter (TSP) was 500 - 600 μg/m^3, and Tura EL-Cement and Helwan Portland cement factories were found to represent 50% of the pollution sources in Helwan region [28]. Then the large percentage in the elements is Si and it is beige size and fall under Mei scattering and an atmosphere containing 200 μg/m^3 is very clear and an atmosphere containing 800 μg/m^3 is much polluted [11].

Figure 12 shows the variations of temperature (˚C) and relative humidity (RH, %) values for three days (21 June as the eclipse day) and the two days before (20 June) and after (22 June) the eclipse day from sunrise to sunset. It would be clear, that the temperature on the day of the eclipse is higher than the day before and the day after it, and vice versa with respect to the relative humidity. Figure 13 shows the change in both temperature (˚C) and RH (%) with respect to time for the three sequence days, the day of the eclipse (21 June, including the duration of the eclipse), the day before (20 June) and the day after (22 June) for the interval time 5.5 h to 12.5 h am. He notes the regular change of both temperature and relative humidity on 20 and 22 June. While the change was irregular on June 21, especially the change in temperature immediately after the time of the eclipse, then followed by a change in the RH.

Table 5. The linear regression between the LT, β and W with the time (hour) and the correlation coefficients (CC) according to Table 4.

Y	a	b	X	CC
LT	0.4941	+0.3313	hour	0.957
β	−0.11389	+0.01697	hour	0.9
W	3.3293	−0.0751	hour	0.828

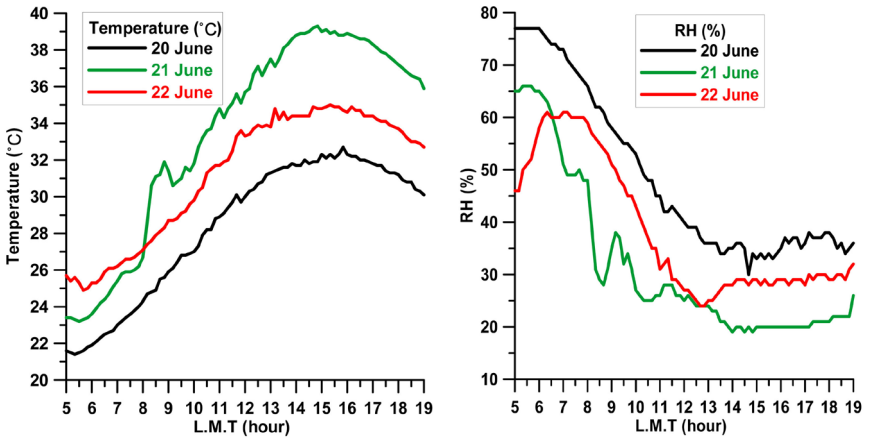

Figure 12. The variation of the temperature (˚C) and RH (%) values for three days (21 June as the eclipse day and the two days before (20 June) and after (22 June) the eclipse day from sunrise to sunset.

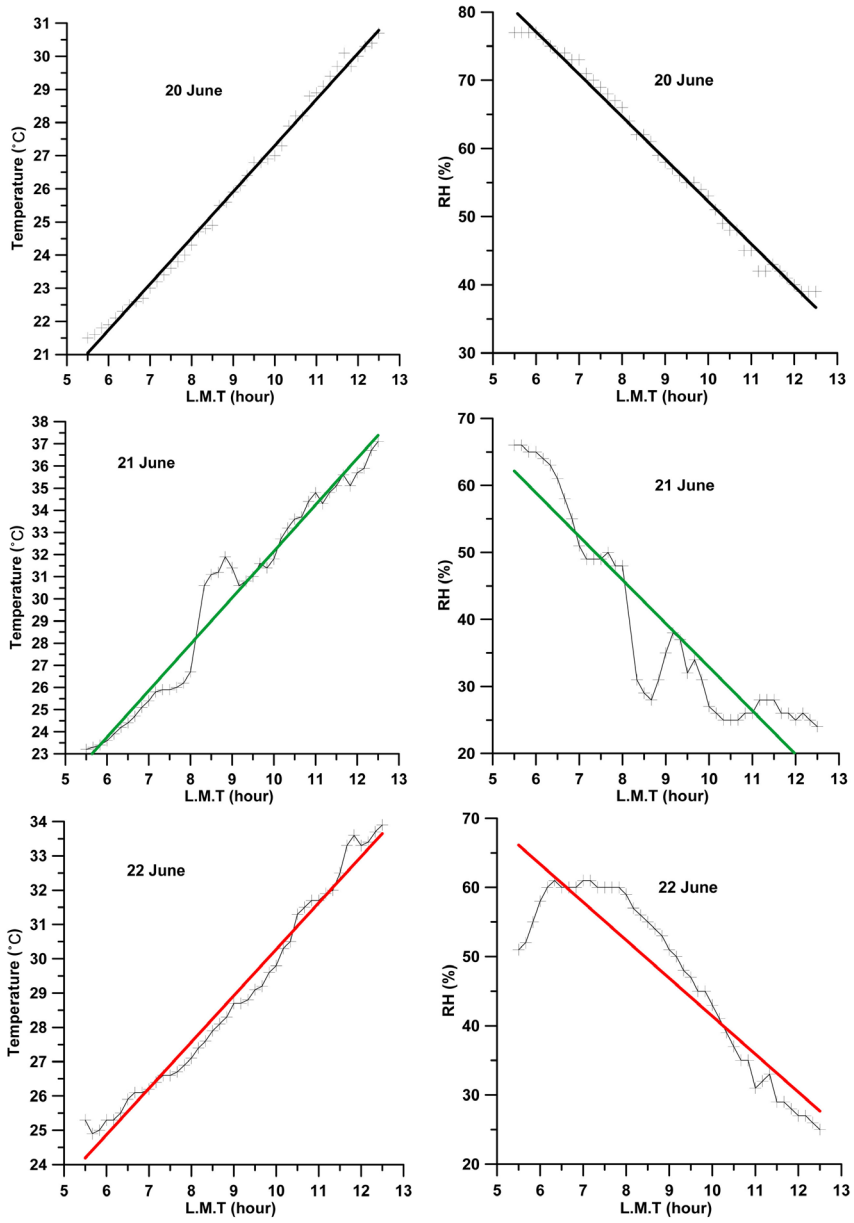

Figure 13. The change in both temperature (˚C) and RH (%) with respect to the time for three sequence days, the day of the eclipse (21 June, including the duration of the eclipse), the day before (20 June) and the day after (22 June) for the interval time 5.5 h to 12.5 h am.

5. Conclusion

The objective of this research is performance of incoming solar radiation components in partial annular solar eclipse on June 21st, 2020, at Helwan, Egypt. The depression is clear at the solar radiation of all components due to the annular solar eclipse, while the depressions of the diffuse and global infrared solar radiation are lower. n all direct radiation compounds (*I*, *Y*, *R* and *IR*) are greatly affected by the eclipse, while the effect is small in the case of total radiation compounds (*G*, G_{uv}, G_{IR} and *D*). The diffuse fraction K_d is higher in the early time,

before the partial eclipse, but during the partial annular eclipse time K_d values are suffers variation and through the day, where the values of K_d lies between K_t and K_{UV}. The clearness indices have higher values during the partial annular eclipse, but after the partial eclipse the values of K_t are higher and the values of K_d are lowest. The IR solar radiation component is predominant outside the partial annular solar eclipse, but these changes during a partial eclipse. The values of direct infrared solar radiation are dominant before and after the partial annular solar eclipse, and also the global infrared solar radiation is dominant. The intensity of color bands as the $W \cdot m^{-2} \cdot nm^{-1}$ are *DIB*3 > *DIB*2 > *DIB*4, and *DIB*1 is opposite direction with *DIB*3 and *DIB*2, the highest intensity is direct red and the lowest intensity is the direct infrared. The different percentage of the color portion bands, *DCBi* ($\%\cdot nm^{-1}$) shows the prevailing color portion bands are *DCB*3 > *DCB*2 > *DCB*4, and *DCB*1 is opposite direction with *DCB*3 and *DCB*2, where the high percent of color portion bands generally are the red color (*DCB*3). The direction and behavior of all colors percent ($\%\cdot nm^{-1}$) are in the same phase, unlike the behavior of colors before and after the eclipse. The highest values of extinction coefficient in G_{IR} solar radiation and the lowest values occur in G_{UV} solar radiation, while the values for G solar radiation occur between them. And the all values of extinction coefficient in the total direct solar radiation and the color bands are nearest them. In general trend, the values of extinction coefficient during the partial eclipse are increasing, while the minimum values of extinction coefficient occur at noon time due to the air mass is less value in the noon. The highest value for the transparency is G_{UV} rays and the lowest is *CB*2. The Linke Turbidity (*LT*) and Angstrom turbidity (β) values are higher in the afternoon than in the morning. This is because of the high temperature in the afternoon, which expands and excites the gases and the dust in the atmosphere. During the eclipse (from the first contact to the last contact), the ranged values of the LT, β and W (cm) are: 2.02 - 3.12, 0.015 - 0.027 and 3.14 - 2.68 respectively. The rate increase of the (*LT*) with time is $\mathrm{d}LT/\mathrm{d}t = +0.3313$, the rate increase of ($\beta$) with the time is $\mathrm{d}\beta/\mathrm{d}t = +0.01697$, while the rate decrease for the W (cm) with the time is $\mathrm{d}W/\mathrm{d}t = -0.0751$. It is clear that the relationship is positive with the progression of time with an increase in the intensity of solar radiation and then the direct functions in the temperature, which leads to an increase in the spread and excitation of the atmospheric air components in a tropospheric region. The relationship is inverse and indirect in case the perceptible water (W, cm) with the time. The regular change of both temperature and relative humidity on 20 and 22 June, while the change was irregular on June 21, especially the change in temperature immediately after the time of the eclipse, then followed by a change in the *RH*.

Conflicts of Interest

The authors declare no conflicts of interest regarding the publication of this paper.

References

[1] Anderson, R.C., Keefer, A.R. and Myers, O.E. (1972) Atmospheric Pressure and Temperature Changes during the 7 March 1970 Solar Eclipse. *Journal Atmosphere Science*, **29**, 583-587. https://doi.org/10.1175/1520-0469(1972)029<0583:APATCD>2.0.CO;2

[2] Petkov, B., Vitale, V., Tomasi, C., Bonafe, U., Scaglione, S., Flori, D., Santaguida, R., Gausa, M., Hansen, G. and Colombo, T. (2006) Narrow-Band Filter Radiometer for Ground-Based Measurements of Global UV Solar Irradiance and Total Ozone. *Applied Optics*, **45**, 4383-4395. https://doi.org/10.1364/AO.45.004383

[3] Duif, P.C. (2004) A Review of Conventional Explanations of Anomalous Observations during Solar Eclipses. http://arxiv.org/ftp/gr-qc/papers/0408/0408023.pdf

[4] Tsakalis, N., Tzortziou, M., Vahamidis, P., Papathanassiou, E. and Karamanos, A. (2008) Eclipse Effects on Field Crops and Marine Zooplankton: The 29 March 2006 Total Solar Eclipse. *Atmospheric Chemistry and Physics*, **8**, 4665-4676. https://doi.org/10.5194/acp-8-4665-2008

[5] Kazadsis, S., Bais, A., Blumthaler, M., Webb, A., Kouremeti, N., Kift, R., Schallhart, B. and Kazantzidis, A. (2007) Effects of Total Solar Eclipse of 29 March 2006 on Surface Radiation. *Atmospheric Chemistry and Physics*, **7**, 9235-9258. https://doi.org/10.5194/acpd-7-9235-2007

[6] Emde, C. and Mayer, B. (2007) Simulation of Solar Radiation during a Total Eclipse: A Challenge for Radiative Transfer. *Atmospheric Chemistry and Physics*, **7**, 2259-2270. https://doi.org/10.5194/acp-7-2259-2007

[7] Mollmann, K.P. and Vollmer, M. (2006) Measurements and Predictions of the Illuminance during a Solar Eclipse. *European Journal of Physics*, **27**, 1299-1314. https://doi.org/10.1088/0143-0807/27/6/004

[8] Koepke, P., Reuder, J. and Schween, J. (2001) Spectral Variation of the Solar Radiation during an Eclipse. *Meteorologische Zeitschrift*, **10**, 179-186. https://doi.org/10.1127/0941-2948/2001/0010-0179

[9] Petkov, B., Tomasi, C., Vitale, V., di Sarra, A., Bonasoni, P., Lanconelli, C., Benedetti, E., Sferlazzo, D., Dimoz, H., Agnesod, G. and Santaguida, R. (2010) Ground-Based Observations of Solar Radiation at Three Italian Sites, during the Eclipse of 29 March, 2006: Signs of the Environment Impact on Incoming Global Irradiance. *Atmospheric Research*, **96**, 131-140. https://doi.org/10.1016/j.atmosres.2009.12.006

[10] Madronich, S. (1993) UV Radiation in the Natural and Perturbed Atmosphere. In: Tevini, M., Ed., *Environmental Effects of UV* (*Ultraviolet*) *Radiation*, Lewis, Boca Raton, 17-69.

[11] Iqbal, M. (1983) An Introduction to Solar Radiation. Academic Press, Cambridge.

[12] Abbott, W.N. (1958) On Certain Radiometric Effects during the Partial Solar Eclipse of February 25, 1952. *Geofis*, *Pura e Applicada* (*Milan*), **39**, 186-193. https://doi.org/10.1007/BF02001144

[13] Rahoma, A.U. and Hassan, A.H. (2007) Fourier Transforms Investigation of Global Solar Radiation at True Noon: In the Desert Climatology. *American Journal of Applied Sciences*, **4**, 902-907. https://doi.org/10.3844/ajassp.2007.902.907

[14] Rahoma, A.U., Shaltout, M.A. and Hassan, A.H. (2004) Study of Spectral Global Solar Radiation during the Partial Solar Eclipse of 11 August, 1999 at Helwan, Egypt. *Journal of Astronomy Society of Egypt*, **12**, 31-45.

[15] Hassan, A.H., Shaltout, M.A. and Rahoma, U.A. (2004) The Depression of Different Solar Radiation Components during the Solar Eclipse, 11 August 1999 over Egypt.

Journal of Astronomy Society of Egypt, **12**, 70-81.

[16] Espenak, F. and Anderson, J. (2004) Total Solar Eclipse of 2006 March 29 (NASA/TP, 212762, 2004).

[17] Carapiperis, L. and Karapiperis, N. (1959) On the Variation of Solar Radiation and Blueness of the Sky during the Eclipse of June 30, 1954 at Athens. *Pure and Applied Geophysics*, **43**, 323-328. https://doi.org/10.1007/BF01993569

[18] Copaciu, V. and Yousef, S.M. (1999) Some Atmospheric Responses the 11 August 1999 Total Solar Eclipse near Bucharest. *Romanian Astronomical Journal*, **9**, 19-23.

[19] Rahoma, A.U., Shaltout, M.A. and Hassan, A.H. (1999) Study of Spectral Global Solar Radiation during the Partial Solar Eclipse of 11 August 1999 at Helwan, Egypt. *Journal of Astronomy Society of Egypt*, **12**, 31-45.

[20] Blumthaler, M., Bais, A., Webb, A., Kazadzis, S., Kift, R., Kouremeti, N., Schallhart, B. and Kazantzidis, A. (2006) Variations of Solar Radiation at the Earth's Surface during the Total Solar Eclipse of 29 March 2006. *Proceedings of the SPIE Conference*, *Remote Sensing* 2006, Stockholm, 11-14 September 2006, Session 3, 37. https://doi.org/10.1117/12.689630

[21] Dani, K.K. and Devara, P.C.S. (2002) Aerosol Optical Depth and Ozone Variations during the Total Solar Eclipse of 24 October, 1995. *Atmospheric Research*, **65**, 1-15. https://doi.org/10.1016/S0169-8095(02)00143-6

[22] Koepke, P., Reuder, J. and Schween, J. (2001) Spectral Variation of the Solar Radiation during an Eclipse. *Meteorologische Zeitschrift*, **10**, 179-186. https://doi.org/10.1127/0941-2948/2001/0010-0179

[23] Zerefos, C., Balis, D.S., Meleti, C., Bais, A.F., Tourpali, K., Kourtidis, K., Vanicek, K., Capelani, F., Kaminski, U., Colombo, T., Stubi, R., Manea, L., Formenti, P. and Andreae, M.O. (2000) Changes in Surface Solar UV Irradiances and Total Ozone during the Solar Eclipse of August 11, 1999. *Journal of Geophysical Research*, **105**, 26463-26473. https://doi.org/10.1029/2000JD900412

[24] Fuchs, E.C., Qudakker, G., Justinek, M. and Dyer, N. (2019) Solar Eclipses and the Surface Properties of Water. *Earth*, *Moon*, *and Planets*, **123**, 15943. https://doi.org/10.1007/s11038-019-09529-0

[25] Hassan, A.H., Rahoma, U.A., Sabry, M. and Fathy, A.M. (2005) Color Portion of Solar Radiation in the Partial Annular Solar Eclipse October 3rd, 2005, at Helwan, Egypt. *Acta Polytechnica*, **50**, 32-40.

[26] Hassan, A.H. and Rahoma, U.A. (2010) Solar Radiation at Total Solar Eclipse, 29 March 2006, at Tobruq. *American Journal of Environmental Science*, **6**, 449-454. https://doi.org/10.3844/ajessp.2010.449.454

[27] Harrison, R.G., Marlton, G.J., Williams, P.D. and Nicoll, K.A. (2015) Coordinated Weather Balloon Solar Radiation Measurements during a Solar Eclipse. *Philosophical Transactions of the Royal Society A*: *Mathematical*, *Physical and Engineering Sciences*, **374**, 221. https://doi.org/10.1098/rsta.2015.0221

[28] Rahoma, U.A., Khalaf, G.M.G., Hashem, H.M. and El-Hagary, M. (2018) X-Ray Diffraction and Fluorescence Analysis for the Suspended Particulate Matter in an Atmospheric Industrially Polluted Region. *International Sixth Conference Sustainable Development and Arab Economic Security*, Cairo, Vol. 34.

[29] Kasten, F. (1980) A Simple Parameterization of the Pyrheliometric Formula for Determining the Linke Turbidity Factor. *Meteor. Rdsch*, **33**, 124-127.

[30] Elminir Hamdy, K., Rahoma, U.A. and Benda, V. (2001) Comparison between Atmospheric Turbidity Coefficients of Desert and Temperate Climates. *Acta Polytechnica*, **41**, 48-59.